Prepublished copy

Nature Environment & Pollution Technology

This is a peer-reviewed prepublished version of the paper

Original Research

Remote Sensing and Machine Learning Approaches for Assessing Environmental Dynamics in the Southeastern Watersheds of Madre de Dios, Peru

Americo Arizaca-Avalos[1], Fidel Huisa-Mamani[2]†, Emmanuel Hernan Tumy-Gomez[3], Wilber Pastor-Contreras[4], Yesenia Fátima Llanque-Añacata[5]

[1]Universidad Nacional del Altiplano, ORCID: 0000-0002-0424-0138

[2] Universidad Nacional del Altiplano, ORCID: 0000-0002-6362-9661

[3] Universidad Nacional del Altiplano, ORCID: 0000-0002-5498-6296

[4] Universidad Nacional del Altiplano, ORCID: 0000-0002-5723-0697

[5] Universidad Nacional del Altiplano, ORCID: 0009-0001-6751-2663

†Corresponding author: Fidel Huisa-Mamani; odinlab322@gmail.com

Key Words	Environment, Remote sensing, Machine learning, NDVI, NDWI
DOI	https://doi.org/10.46488/NEPT.2025.v24i04.D1783 (DOI will be active only after the final publication of the paper)
Citation for the Paper	Arizaca-Avalos, A., Huisa-Mamani, F., Tumy-Gomez, E.H., Pastor-Contreras, W. and Llanque-Añacata, Y.F., 2025. Remote sensing and machine learning approaches for assessing environmental dynamics in the Southeastern Watersheds of Madre de Dios, Peru. *Nature Environment and Pollution Technology*, 24(4), p. D1783. https://doi.org/10.46488/NEPT.2025.v24i04.D1783

ABSTRACT

This study evaluates environmental changes in the southeastern basins of Madre de Dios, Peru, using multi-spectral remote sensing and machine learning techniques. Landsat and Sentinel imagery were processed to compute the Normalized Difference Vegetation Index (NDVI) and Normalized Difference Water Index (NDWI). Principal Component Analysis was employed for dimensionality reduction, while unsupervised K-means clustering was used to classify land cover. Results reveal a marked reduction in dense vegetation alongside growing extents of bare soil and water bodies, underscoring the effectiveness of our approach for comprehensive environment monitoring and change detection.

INTRODUCTION

The Environmental degradation in Madre de Dios, Peru, has been associated with phenomena such as deforestation, soil erosion, and water contamination with heavy metals (Cuya et al. 2021; Velásquez Ramírez et

al. 2020). Although economic incentives may promote the expansion of these informal activities (Cuya et al. 2021; Sanguinetti, 2020), previous studies in Madre de Dios have documented extensive deforestation, biodiversity loss, soil degradation, and water pollution (Cuya et al. 2021; Velásquez Ramírez et al. 2020; Diringer et al. 2015). However, establishing a direct causal link between these environmental changes and informal mining practices remains an area for further investigation, especially given the region's complex socioeconomic dynamics that challenge mitigation efforts (Cuya et al. 2021; Sanguinetti, 2020).

Advances in remote sensing and machine learning (ML) now enable detailed analyses of land cover and vegetation health using multispectral imagery (Camps-Valls, 2009; Kopačková-Strnadová et al. 2024; Liu et al. 2024). Techniques such as Support Vector Machines (SVM), Random Forests (RF), and Gradient Boosted Decision Trees (GBDT) have demonstrated high accuracy in environmental classification and pre-diction (Nalepa, 2021; Potić et al. 2023), facilitating real-time monitoring and environmental management (Alotaibi & Nassif, 2024; Liu et al. 2024).

However, the comprehensive application of these methods to evaluate the environmental impacts of informal mining in Madre de Dios remains limited, as most studies have focused on the direct effects of mercury and socioeconomic aspects (Cuya et al. 2021; Diringer et al. 2015). This study addresses that gap by employing multispectral analysis enhanced by ML to identify evidence of vegetation and hydrological degradation in the southeastern basins of Madre de Dios, following established standards (Alotaibi & Nassif, 2024; Dios-Castillo et al. 2024).

2. MATERIALS AND METHODS

2.1. Subsection

The study was carried out in the southeastern watersheds of Madre de Dios, Peru (Fig. 1), a tropical region averaging 24.5 °C and 2,800 mm of annual precipitation (Wang et al. 2023). This biodiverse area, home to vast Amazonian forests, faces severe anthropogenic pressures from illegal mining and deforestation (Csillik & Asner, 2020; Markham & Sangermano, 2018).

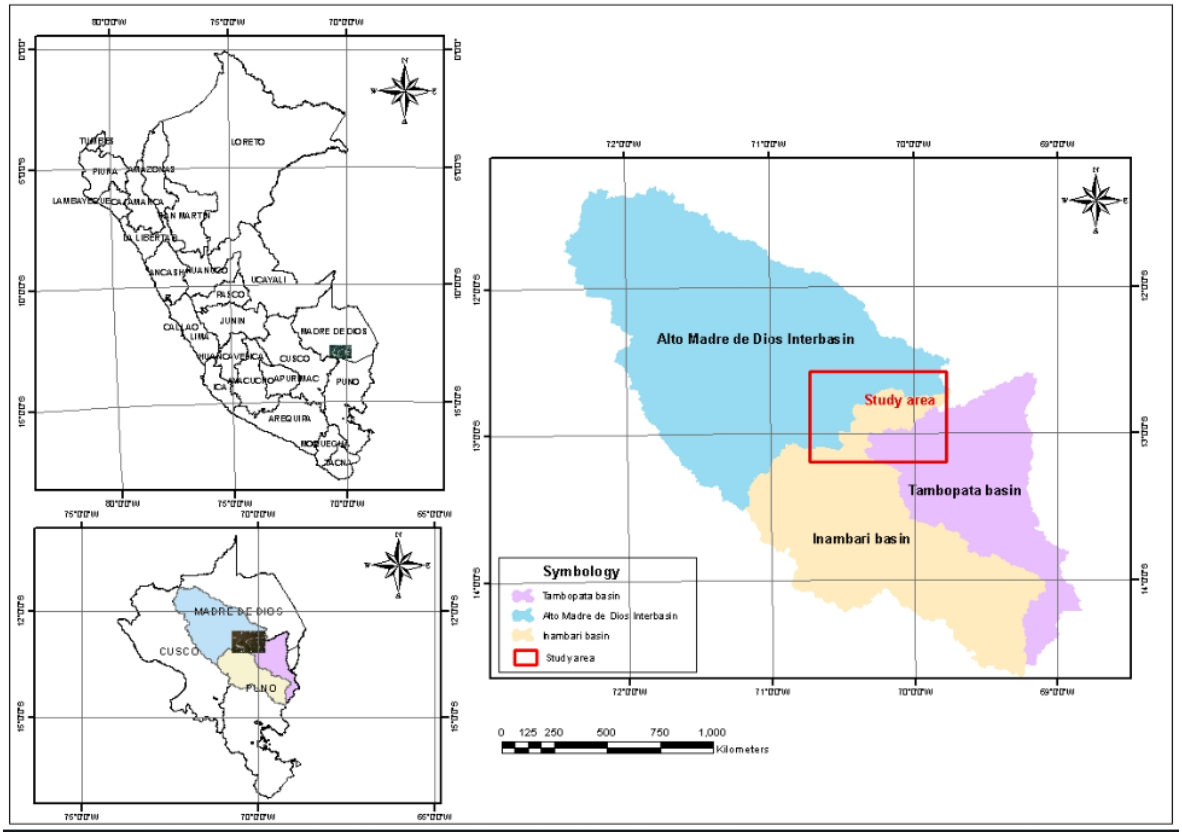

Fig. 1: Study area in the southeastern Madre de Dios region, Peru; Alto Madre de Dios, Tambopata, and Inambari basins.

2.2. Satellite Image Selection and Preprocessing

This study ensured high spatial resolution and temporal consistency by using multispectral images from Landsat 5 (TM) in 2003 and Landsat 8 (OLI/TIRS) in 2022, supplemented with Sentinel-2 (MSI) for its enhanced spectral capabilities. Sensors were selected based on free availability, low cloud cover (<10%), and consistent temporal coverage, with all images sourced from the USGS Earth Explorer for uniform quality. Preprocessing included radiometric and atmospheric corrections (using SNAP: Sen2Cor for Sentinel-2 and DOS for Landsat 8), clipping to the study area via SINAFOR watershed shapefiles, and reprojecting to UTM Zone 19S. Table 1 provides the satellite image specifications.

Table 1: Specifications of satellite images used in the study.

Platform	Sensor	Bit Depth	Spatial Resolution (m)	Spectral Resolution	Frequency	Coverage
Landsat 5	TM	8 bits	30	7 bands	16 days	180 km × 180 km
Landsat 8	OLI/TIRS	16 bits	30(B8:15m)	11 bands	16 days	185 km × 185 km

2.3. Environmental Index Calculation

Two spectral indices were calculated using the corresponding satellite image bands: the Normalized Difference Vegetation Index (NDVI) and the Normalized Difference Water Index (NDWI). NDVI was employed to estimate vegetation density, calculated using the standard formula, as also applied by Jeevalakshmi et al. (2016).

$$NDVI = \frac{NIR - RED}{NIR + RED}$$

where NIR and RED correspond to the near-infrared and red bands, respectively.

NDWI was used to assess hydrological features, calculated using the following formula, as applied in recent studies such as Assiri et al. (2024).

$$NDWI = \frac{NIR - SWIR}{NIR + SWIR}$$

where NIR represents the near-infrared band (0.76–0.90 μm for Landsat 5 TM; 0.85–0.88 μm for Landsat 8 OLI) and SWIR represents the shortwave infrared band (1.55–1.75 μm for Landsat 5 TM; 1.57–1.65 μm for Landsat 8 OLI).

2.4. Dimensionality Reduction and Land Cover Classification

PCA was applied to Bands 1, 2, and 3 from Landsat 5 (2003) and Landsat 8 (2022) imagery to reduce dimensionality and extract key spectral features. For land cover classification, unsupervised K-means clustering was used on NDVI and NDWI indices to segment the area into ecologically relevant categories. Optimal parameters were determined via the elbow method (Ketchen & Shook, 1996) and silhouette analysis (Rousseeuw, 1987), testing K values from 2 to 10, with a maximum of 10 iterations and a 5% convergence threshold.

2.5. Vegetation Classification and Land Cover Dynamics

NDVI thresholds were defined to classify vegetation into five categories, capturing variations in density and ecological significance. This approach allowed for detailed assessments of vegetation health and spatial distribution. The NDVI ranges and corresponding ecological interpretations are as follows:

Table 2: Specifications of satellite images used in the study.

NDVI Range	Class	Category	Ecological Interpretation
-1.0 to 0.2	1	Non-vegetated	Bare soil, mining areas, water bodies
0.2 to 0.4	2	Sparse vegetation	Recently disturbed areas, early succession
0.4 to 0.6	3	Moderate vegetation	Secondary forest, regenerating areas
0.6 to 0.8	4	Dense vegetation	Established forest, mature vegetation
0.8 to 1.0	5	Very dense vegetation	Primary forest, optimal canopy condition

Land cover changes (2003–2022) were evaluated by comparing vegetation categories, revealing deforestation, vegetation loss, and hydrological shifts. NDVI and NDWI metrics (mean, standard deviation, total area) quantified these changes. PCA reduced dimensionality, K-means classified land cover, and temporal analysis examined vegetation and hydrology. R and ArcGIS ensured reproducibility and provided critical insights into environmental change.

3. RESULTS

3.1. Principal Component Analysis (PCA)

The Principal Component Analysis (PCA) applied to spectral Bands 1, 2, and 3 of Landsat 5 (2003) and Landsat 8 (2022) highlighted significant variability in the study area's spectral features. The results, shown in Fig. 2, reveal differences in land cover characteristics between the two years analyzed.

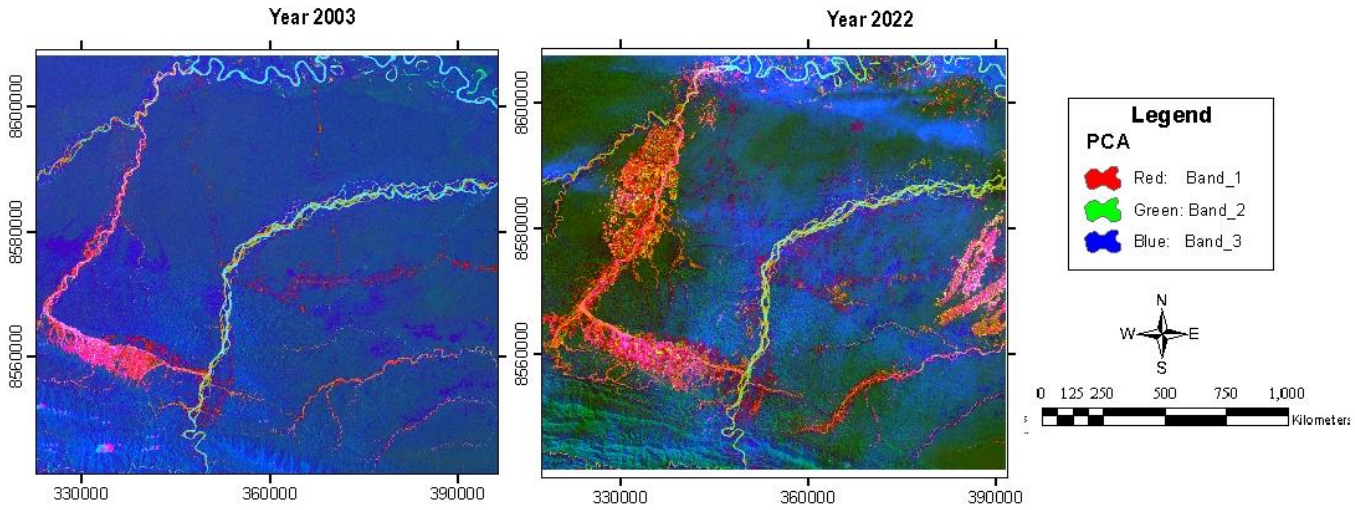

Fig. 2: Differences of Principal Component Analysis (PCA).

In 2003, the first three principal components explained 95.60% of the variance (with PC1 capturing 64.03% and standard deviations of 2.1171, 1.1789, and 0.9055 for PC1, PC2, and PC3, respectively), confirming effective dimensionality reduction and distinct spectral patterns in the dataset.

Table 3: Analysis of the distribution and variability of PCA data.

Importance of Principal Components						
	Year 2003			Year 2022		
	PC1	**PC2**	**PC3**	**PC1**	**PC2**	**PC3**
Standard deviation	2.1171	1.1789	0.9055	2.6477	1.2880	1.1749
Proportion of variance	0.6403	0.1986	0.1171	0.6373	0.1508	0.1255
Cumulative proportion	0.6403	0.8388	**0.956**	0.6373	0.7881	**0.9136**

For 2022, PC1 explained 63.73% of the total variance, with slightly higher standard deviations for PC1 (2.6477) and PC2 (1.2880), while PC3 showed a standard deviation of 1.1749. The cumulative variance for 2022 was 91.36%, slightly lower than in 2003, which may reflect increased complexity or heterogeneity in the spectral data due to changes in land cover.

3.2. Normalized Difference Vegetation Index (NDVI)

The NDVI analysis revealed substantial changes in vegetation density and health between 2003 and 2022. In 2003, areas with high vegetation density (NDVI > 0.6) covered approximately 68% of the total area, while

in 2022, this percentage decreased to 61%. These variations suggest a loss of dense vegetation, particularly in regions adjacent to mining activities.

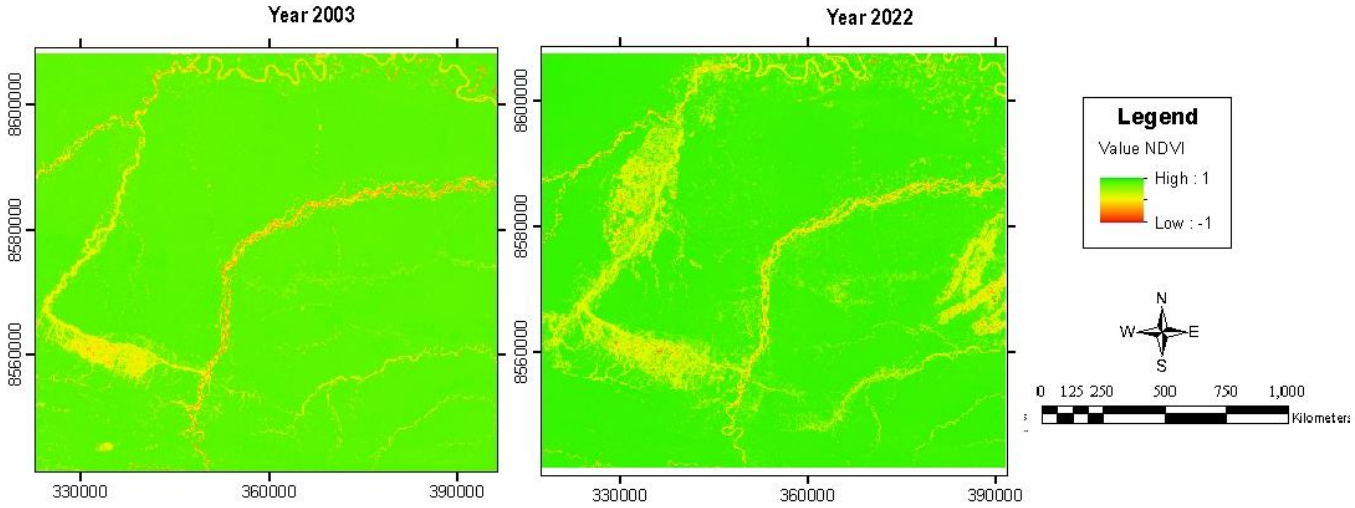

Fig. 3: Normalized Difference Vegetation Index (NDVI).

Fig. 3 presents the Normalized Difference Vegetation Index (NDVI) for the years 2003 and 2022. NDVI is a key measure for assessing vegetation health in a specific region. In the map, NDVI values are represented using a color gradient: green indicates areas with high density of healthy vegetation, while yellow and orange tones reflect areas with lower vegetation density or bare soils.

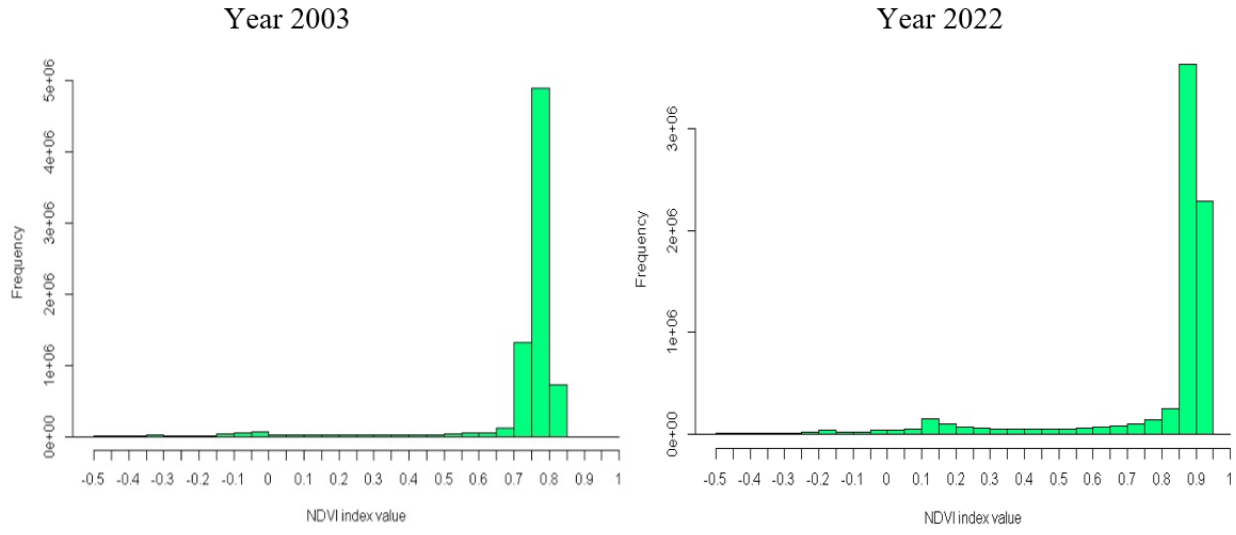

Fig. 4: NDVI Pixel Value Distribution.

3.3. Normalized Difference Vegetation Index (NDVI)

The NDVI Pixel Value Distribution shown in Fig. 4 between 2003 and 2022 shows a shift from a highly concentrated distribution with a peak at 0.7-0.9 (frequency ~4e+06) to a pattern with two prominent peaks at 0.8-1.0 (frequency ~3e+06), indicating subtle changes in vegetation structure over the study period.

The raster dimensions for NDVI analysis covered similar spatial extents shown in Table 4, the mean NDVI increased from 0.725 in 2003 to 0.799 in 2022, with the standard deviation rising from 0.184 to 0.242, indicating a higher heterogeneity in vegetation cover.

Table 4: Raster dimension NDVI.

Metrics	Year 2003	Year 2022
Average	0.725	0.799
Minimum	-1	-1
Maximum	1	1
Standard deviation	0.184	0.242
Row	2233	2198
Column	3418	3396
Total pixel	7632394	7464408
Spatial resolution	30	30
Area m^2	6869154600	6717967200
Area Ha	686915.46	671796.72

3.4. Normalized Difference Water Index (NDWI)

The NDWI frequency distribution as shown in Fig. 5, display ranges from approximately -0.5 to 0.5. Most values are clustered around 0, indicating an intermediate water content in the vegetation.

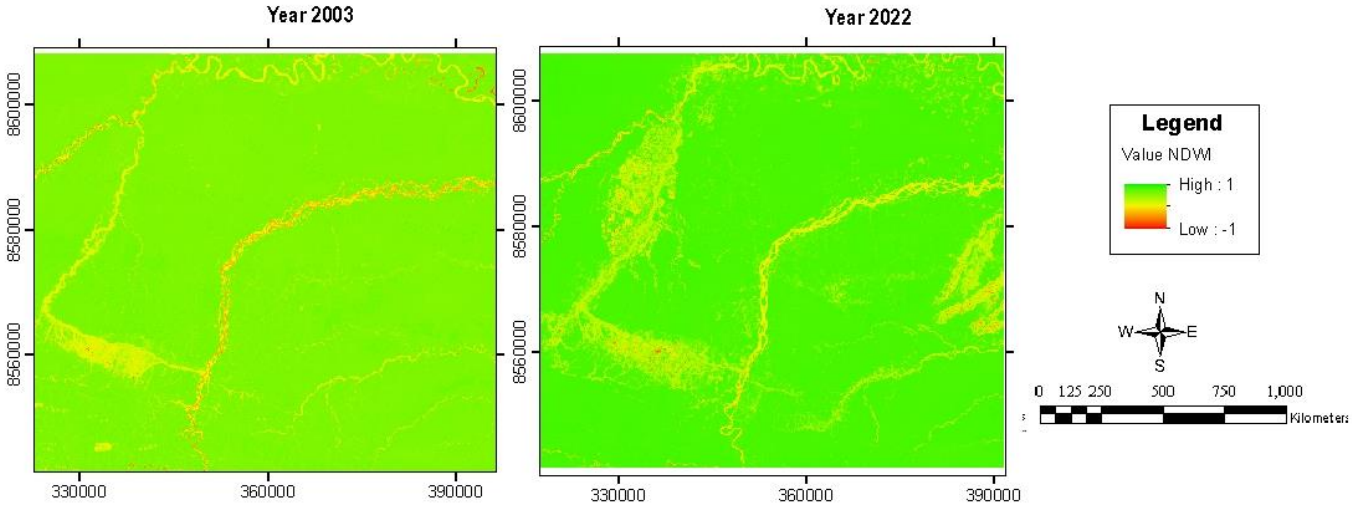

Fig. 5: Normalized Difference Water Index (NDWI).

Furthermore, Fig. 6 shows the highest frequency just above -0.5, indicating a high concentration of pixels with this NDWI value, which suggests areas with relatively low water content. In summary, NDWI values near zero indicate moderate water presence in the vegetation, while the predominance of values around -0.5 reinforces the existence of regions with limited water content.

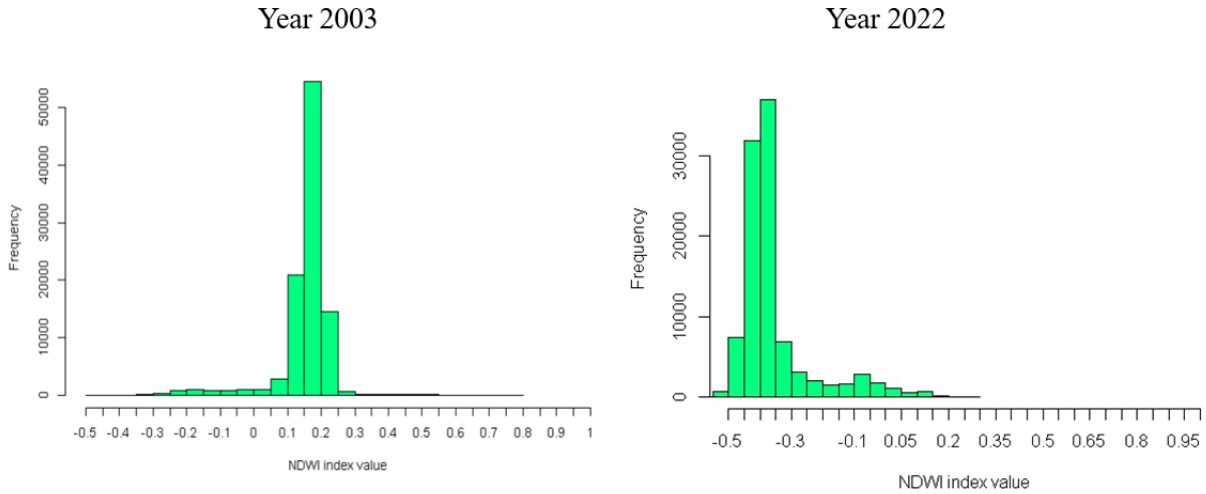

Fig. 6: Normalized Difference Water Index (NDWI).

A two-dimensional scatter plot with a color scale from 0.9990 to 1.0010 encodes a water-related variable (Fig. 7). The distribution of points forms clusters and linear features corresponding to geographic entities such as riverbanks or shorelines, indicating a strong spatial correlation between location and water characteristics. Regions with values near 1 denote a high-water concentration, signifying greater water content in those areas.

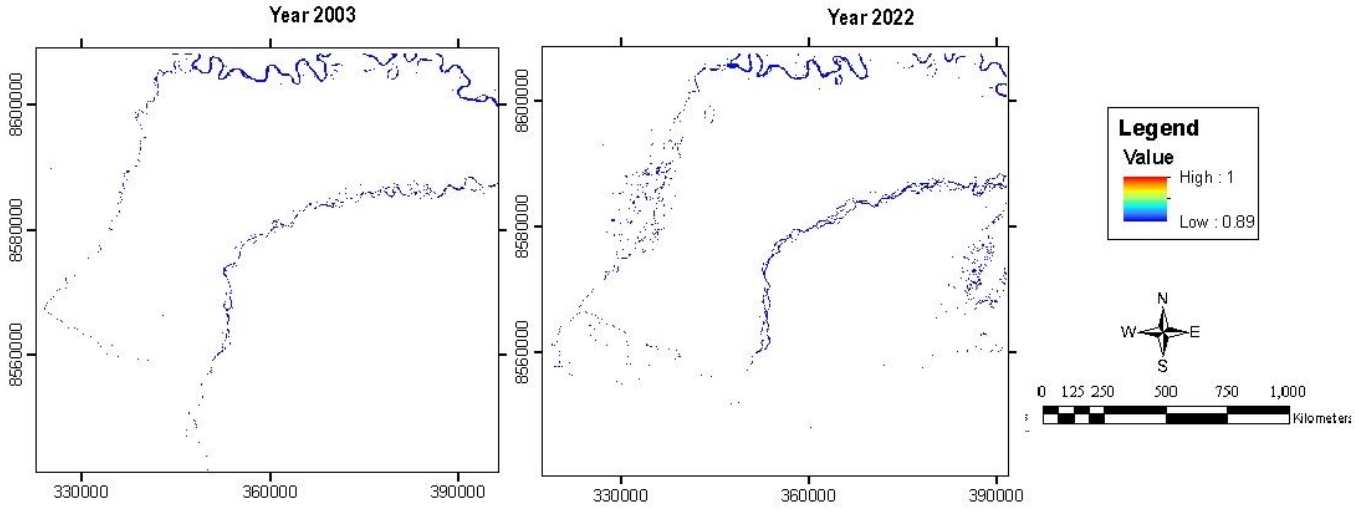

Fig. 7: Normalized Difference Water Index (NDWI).

The comparative data (Table 5) reveal that between 2003 and 2022, the mean increased from 0.125 to 0.341 while the minimum and maximum remained constant at -1 and 1. Additionally, the standard deviation rose from 0.090 to 0.115, indicating increased variability, and the measured area decreased from 6,869,154,600 m² (686,915.46 ha) to 6,717,967,200 m² (671,796.72 ha). These findings indicate a complex and dynamic scenario, with improvements in some aspects and significant declines in others.

Table 5: Raster dimension NDWI.

Metrics	Year 2003	Year 2022
Average	0.125	0.341
Minimum	-1	-1
Maximum	1	1
Standard deviation	0.090	0.115
Row	2233	2198
Column	3418	3396
Total pixel	7632394	7464408
Spatial resolution	30	30
Area m^2	6869154600	6717967200
Area Ha	686915.46	671796.72

Likewise, Table 6 illustrates that water body areas expanded from approximately 67.36 million m² (~6,735.87 ha) in 2003 to about 100.73 million m² (~10,073.16 ha) in 2022, likely reflecting changes in land use and hydrological dynamics.

Table 6: Water body areas – NDWI.

Description	Year 2003		Year 2022	
	m^2	Ha	m^2	Ha
Water body areas	67358700	6735.87	100731600	10073.16

3.5. Land Cover Classification Using K-means

K-means classified land cover for 2003 and 2022 (Fig. 8), distinguishing healthy vegetation (green), bare soil (yellow), and water bodies (blue). Healthy vegetation declined, while bare soil and water bodies increased, consistent with NDWI results and suggesting land degradation, conversion, and increased surface water from artificial reservoirs or land use changes.

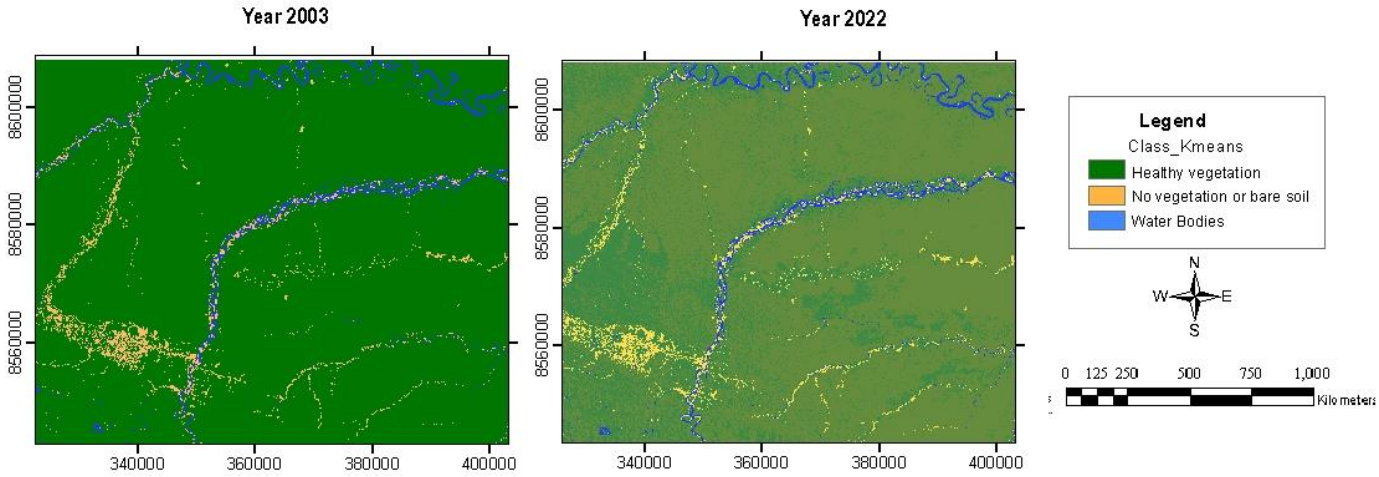

Fig. 8: Classification Kmeans.

The land use classification (Table 7) shows that between 2003 and 2022, healthy vegetation declined from 648,155.34 ha (94.36%) to 568,445.94 ha (84.62%), bare soil increased from 23,360.4 ha (3.40%) to 75,847.77 ha (11.29%), and water bodies expanded from 15,399.72 ha (2.24%) to 27,503.01 ha (4.09%).

Table 7: Areas Classified According to K-means.

Classification	Year 2003		Year 2022	
	Ha	%	Ha	%
Healthy Vegetation	648155.34	94.36%	568445.94	84.62%
Non-Vegetated or Bare Soil	23360.4	3.40%	75847.77	11.29%

Water Bodies	15399.72	2.24%	27503.01	4.09%

3.6. Statistical Evidence of NDVI and NDWI Change

Table 4 summarizes the inferential statistics. Mean NDVI increased from 0.725 ± 0.184 in 2003 to 0.799 ± 0.242 in 2022, a rise of +0.074 (95 % CI = 0.073 – 0.075). Welch's unequal-variance t-test confirmed the shift as highly significant, t (32 421) = 147.8, $p < 0.001$; the non-parametric Mann-Whitney U test corroborated this result ($U = 4.52 \times 10^{12}$, $p < 0.001$). Effect-size metrics (Cohen's $d = 0.80$; Cliff's $\delta = 0.49$) point to a pronounced shift, signaling a biologically significant decline in vegetation vitality.

NDWI exhibited an even stronger shift, rising from 0.125 ± 0.090 to 0.341 ± 0.115 ($\Delta = +0.216$; 95 % CI = 0.215 – 0.217). Welch's test yielded t (32 143) = 403.6, $p < 0.001$, while the Mann-Whitney test produced $U = 5.77 \times 10^{12}$, $p < 0.001$. The associated effect size is very large (Cohen's $d = 1.68$; Cliff's $\delta = 0.86$), indicating a substantial alteration in surface-water signatures over the study period.

Table 8: Statistical Comparison of NDVI and NDWI Indices.

Index	Year-1 Mean ± SD	Year-2 Mean ± SD	Δ (95 % CI)	Welch *t*	*p*	Cohen's *d*	Mann-Whitney *U*	Cliff's δ
NDVI	0.725 ± 0.184	0.799 ± 0.242	+0.074 (0.073–0.075)	147.8	<0.001	0.80	4.52×10^{12}	0.49
NDWI	0.125 ± 0.090	0.341 ± 0.115	+0.216 (0.215–0.217)	403.6	<0.001	1.68	5.77×10^{12}	0.86

4. DISCUSSION

The multi-temporal analysis of land-cover dynamics in Madre de Dios (2003 – 2022) documents a pronounced contraction of healthy forest—from 94.36 % to 84.62 %—accompanied by a tripling of bare-soil extent (from 3.40 % to 11.29 %) and a notable expansion of surface-water bodies (from 6 735.87 ha to 10 073.16 ha). Pixel-scale heterogeneity in NDVI values evidences progressive fragmentation of the residual forest matrix, whereas heightened spatial variability in NDWI denotes an increasingly irregular distribution of surface water. Collectively, these quantitative shifts constitute the empirical foundation for the interpretative discussion that follows.

The observed trajectories are attributable principally to the intensification of artisanal and small-scale gold-mining activities (Asner & Tupayachi, 2017; Caballero Espejo et al., 2018). The steep decline in healthy vegetation signifies escalating anthropogenic pressure, while the broader dispersion of NDVI values indicates habitat discontinuity capable of undermining biodiversity assemblages and perturbing local microclimates (Haddad et al., 2015; Laurance et al., 2014). The enlargement of water bodies accords with the proliferation of min-

ing pits that function as artificial reservoirs (Alvarez-Berríos & Aide, 2015) and may disrupt watershed hydrology while enhancing mercury mobilisation (Diringer et al., 2015; Forsberg et al., 2017). Increased NDWI variability corroborates a fragmented hydrological network characteristic of deforested Amazonian landscapes (Davidson et al., 2012). In concert, the elevated spectral complexity revealed by principal-component analysis and the rise in non-vegetated classes identified through K-means clustering attest to an accelerated trajectory of land degradation consonant with regional observations (Numata et al., 2017).

Methodological consonance is discernible in the work of Pushpalatha et al. (2024), wherein a multi-temporal support-vector-machine framework delineated rapid urban expansion and concomitant vegetational attrition in Mysuru (India) with high classification fidelity, thereby underscoring the epistemic robustness and transferability of advanced remote-sensing and machine-learning protocols across divergent socio-ecological settings.

Mining and infrastructure expansion remain pivotal drivers of environmental degradation in Madre de Dios (Fearnside, 2017; Barber et al., 2014). Road construction facilitates forest conversion by increasing territorial accessibility (Kaimowitz & Smith, 2001) and modulates regional hydrology and local climatic regimes (Lawrence & Vandecar, 2015; Coomes et al., 2017). To mitigate these impacts, stricter mining regulations and conservation incentives, such as payment-for-ecosystem-services programs, are needed (Giudice & Börner, 2024). Community-based conservation efforts have proven effective in reducing deforestation (Schwartzman et al. 2000; Rodrigues et al. 2009). This study underscores the urgent need for stronger environmental policies and sustainable land-use strategies to protect forests and water resources in Madre de Dios.

5. CONCLUSIONS

The study evidences profound environmental transformation in Madre de Dios between 2003 and 2022, characterized by a pronounced contraction of forest cover, an expansion of bare soil, and a measurable increase in surface-water bodies. These trajectories principally attributable to deforestation and illegal gold-mining have disrupted local ecosystems and modified hydrological cycles. The decline in dense, healthy vegetation, manifested in lower NDVI values and shifts in land-cover classifications, testifies to extensive land degradation within this biodiverse tropical region.

The observed rise in bare soil and the enlargement of water bodies not only confirm the loss of natural forest but also point to the creation of artificial reservoirs and altered patterns of water distribution. Such fragmentation of natural habitats undermines biodiversity, perturbs microclimates, and heightens environmental risks, including mercury mobilization from mining activities. While these findings rest on robust remote-sensing diagnostics, they derive from satellite observations alone and from imagery restricted to a single dry-season epoch; future work that incorporates systematic ground-truth verification and multi-season datasets will further

refine thematic accuracy and temporal representativeness without altering the substantive trends identified herein.

Overall, the findings underscore the urgent need for more stringent environmental policies, improved mining regulations, and targeted conservation incentives. Community-based initiatives and sustainable land-use strategies are critical to mitigating further damage and restoring ecological integrity. By combining advanced remote sensing techniques with proactive local engagement, there is a promising pathway toward safeguarding the Amazon's unique environmental heritage for future generations.

Acknowledgments: The authors gratefully acknowledge the support provided by the Universidad Nacional del Altiplano Puno for this project.

Conflicts of Interest: The authors declare no conflicts of interest.

REFERENCES

1. Alvarez-Berríos, N. L. and Aide, T. M., 2015. Global demand for gold is another threat for tropical forests. *Environmental Research Letters*, 10(1), pp.014006. [https://doi.org/10.1088/1748-9326/10/1/014006]
2. Alotaibi, E. and Nassif, N., 2024. Artificial intelligence in environmental monitoring: in depth analysis. Discover Artificial Intelligence, 4(1), pp.84. [https://doi.org/10.1007/s44163-024-00198-1]
3. Assiri, M. E., Ali, M. A., Siddiqui, M. H., AlZahrani, A., Alamri, L., Alqahtani, A. M. and Ghulam, A. S., 2024. Remote sensing assessment of water resources, vegetation, and land surface temperature in eastern Saudi Arabia: identification, variability, and trends. Remote Sensing Applications: Society and Environment, 36, 101296. [https://doi.org/10.1016/j.rsase.2024.101296]
4. Asner, G. P. and Tupayachi, R., 2017. Accelerated losses of protected forests from gold mining in the Peruvian Amazon. Environmental Research Letters, 12(9), pp.094004. [https://doi.org/10.1088/1748-9326/aa7dab]
5. Barber, C. P., Cochrane, M. A., Souza, C. M. and Laurance, W. F., 2014. Roads, deforestation, and the mitigating effect of protected areas in the Amazon. Biological Conservation, 177, pp.203–209. [https://doi.org/10.1016/j.landusepol.2024.107197]
6. Giudice, R. and Börner, J., 2024. Cost effectiveness and income effects of alternative forest conservation policy mixes for the Peruvian Amazon. Land Use Policy, 143, 107197. [https://doi.org/10.1016/j.ecolecon.2017.07.008]
7. Caballero Espejo, J., Messinger, M., Román Dañobeytia, F., Ascorra, C., Fernandez, L. E. and Silman, M., 2018. Deforestation and forest degradation due to gold mining in the Peruvian Amazon: a 34 year perspective. Remote Sensing, 10(12), 1903. [https://doi.org/10.3390/rs10121903]
8. Camps Valls, G., 2009. Machine learning in remote sensing data processing. In: 2009 IEEE International Workshop on Machine Learning for Signal Processing, pp.1–6. [https://doi.org/10.1109/MLSP.2009.5306233]

9. Coomes, D. A., Dalponte, M., Jucker, T., Asner, G. P., Banin, L. F., Burslem, D. F., … and Qie, L., 2017. Area based vs tree centric approaches to mapping forest carbon in Southeast Asian forests from airborne laser scanning data. Remote Sensing of Environment, 194, pp.77–88. [https://doi.org/10.1016/j.rse.2017.03.017]
10. Csillik, O. and Asner, G. P., 2020. Aboveground carbon emissions from gold mining in the Peruvian Amazon. Environmental Research Letters, 15(1), pp.014006. [https://doi.org/10.1088/1748-9326/ab639c]
11. Cuya, A., Glikman, J. A., Groenendijk, J., Macdonald, D. W., Swaisgood, R. R. and Barocas, A., 2021. Socio environmental perceptions and barriers to conservation engagement among artisanal small scale gold mining communities in southeastern Peru. Global Ecology and Conservation, 31, e01816. [https://doi.org/10.1016/j.gecco.2021.e01816]
12. Davidson, E. A., De Araújo, A. C., Artaxo, P., Balch, J. K., Brown, I. F., Bustamante, M. M. C. et al., 2012. The Amazon basin in transition. Nature, 481(7381), pp.321–328. [https://doi.org/10.1038/nature10717]
13. Dios Castillo, C., Chafloque Llontop, C. and Sánchez Rentería, R., 2024. Effectiveness of machine learning in environmental pollution from remote sensing images. In: Proceedings of the LACCEI International Multi conference for Engineering, Education and Technology. [https://doi.org/10.18687/LACCEI2024.1.1.1402]
14. Diringer, S. E., Feingold, B. J., Ortiz, E. J., Gallis, J. A., Araújo Flores, J. M., Berky, A., Pan, W. K. Y. and Hsu Kim, H., 2015. River transport of mercury from artisanal and small scale gold mining and risks for dietary mercury exposure in Madre de Dios, Peru. Environmental Science: Processes & Impacts, 17(2), pp.478–487. [https://doi.org/10.1039/C4EM00567H]
15. Fearnside, P. M., 2017. Deforestation of the Brazilian Amazon. Oxford Research Encyclopedia of Environmental Science. [https://doi.org/10.1093/acrefore/9780199389414.013.102]
16. Forsberg, B. R., Melack, J. M., Dunne, T., Barthem, R. B., Goulding, M., Paiva, R. C. D. et al., 2017. The potential impact of new Andean dams on Amazon fluvial ecosystems. PLOS ONE, 12(8), e0182254. [https://doi.org/10.1371/journal.pone.0182254]
17. Haddad, N. M., Brudvig, L. A., Clobert, J., Davies, K. F., Gonzalez, A., Holt, R. D. et al., 2015. Habitat fragmentation and its lasting impact on Earth's ecosystems. Science Advances, 1(2), e1500052. [https://doi.org/10.1126/sciadv.1500052]
18. Jeevalakshmi, D., Reddy, S. N. and Manikiam, B., 2016. Land cover classification based on NDVI using LANDSAT8 time series: a case study in the Tirupati region. In: International Conference on Communication and Signal Processing, ICCSP 2016, pp.1332–1335. [https://doi.org/10.1109/ICCSP.2016.7754369]
19. Kaimowitz, D. and Smith, J., 2001. Soybean technology and the loss of natural vegetation in Brazil and Bolivia. In: Agricultural Technologies and Tropical Deforestation, pp.195–212. [https://doi.org/10.1079/9780851994512.0195]
20. Ketchen, D. J. and Shook, C. L., 1996. The application of cluster analysis in strategic management research: an analysis and critique. Strategic Management Journal, 17(6), pp.441–458. [https://doi.org/10.1002/(SICI)1097-0266(199606)17:6<441::AID-SMJ819>3.0.CO;2-G]
21. Kopačková Strnadová, V., Kýhos, M. and Jelének, J., 2024. Developing scalable monitoring system for acid mine drainage detection. In: IGARSS 2024 – 2024 IEEE International Geoscience and Remote Sensing Symposium, pp.3404–3408. [https://doi.org/10.1109/IGARSS53475.2024.10641851]
22. Laurance, W. F., Sayer, J. and Cassman, K. G., 2014. Agricultural expansion and its impacts on tropical nature. Trends in Ecology & Evolution, 29(2), pp.107–116. [https://doi.org/10.1016/j.tree.2013.12.001]
23. Lawrence, D. and Vandecar, K., 2015. Effects of tropical deforestation on climate and agriculture. Nature Climate Change, 5(1), pp.27–36. [https://doi.org/10.1038/nclimate2430]

24. Liu, S. S., Zhang, B., Li, X. Y., Xin, L., Ying, G. G. and Chen, C. E., 2024. Recent advances in the application of machine learning in environmental analysis and detection. [Journal Name Not Provided], 43(8), pp.1105–1116. [https://doi.org/10.12452/j.fxcsxb.24052775]
25. Markham, K. E. and Sangermano, F., 2018. Evaluating wildlife vulnerability to mercury pollution from artisanal and small-scale gold mining in Madre de Dios, Peru. Tropical Conservation Science, 11. [https://doi.org/10.1177/1940082918794320]
26. Nalepa, J., 2021. Recent advances in multi and hyperspectral image analysis. Sensors, 21(18), pp.6002. [https://doi.org/10.3390/s21186002]
27. Numata, I., Silva, S. S., Cochrane, M. A., d'Oliveira, M. V. N. and Withey, K., 2017. Fire and edge effects in a fragmented tropical forest landscape in the southwestern Amazon. Forest Ecology and Management, 401, pp.135–146. [https://doi.org/10.1016/j.foreco.2017.07.010]
28. Potić, I., Srdić, Z., Vakanjac, B., Bakrač, S., Đorđević, D., Banković, R. and Jovanović, J. M., 2023. Improving forest detection using machine learning and remote sensing: a case study in southeastern Serbia. Applied Sciences, 13(14), 8289. [https://doi.org/10.3390/app13148289]
29. Pushpalatha, V., Mahendra, H.N., Prasad, A.M., Sharmila, N., Kumar, D.M., Basavaraju, N.M., Pavithra, G.S. and Mallikarjunaswamy, S., 2024. An Assessment of Land Use Land Cover Using Machine Learning Technique. Nature Environment and Pollution Technology, 23(4), pp.2211-2219. [https://doi.org/10.46488/NEPT.2024.v23i04.025]
30. Rodrigues, A. S. L., Ewers, R. M., Parry, L., Souza, C., Verissimo, A. and Balmford, A., 2009. Boom and bust development patterns across the Amazon deforestation frontier. Science, 324(5933), pp.1435–1437. [https://doi.org/10.1126/science.1174002]
31. Rousseeuw, P. J., 1987. Silhouettes: a graphical aid to the interpretation and validation of cluster analysis. Journal of Computational and Applied Mathematics, 20, pp.53–65. [https://doi.org/10.1016/0377-0427(87)90125-7]
32. Schwartzman, S., Moreira, A. and Nepstad, D., 2000. Rethinking tropical forest conservation: perils in parks. Conservation Biology, 14(5), pp.1351–1357. [https://doi.org/10.1046/j.1523-1739.2000.99329.x]
33. Sanguinetti, S., 2020. Fostering social change in Peru through communication: the case of the Manuani Miners Association. In: Handbook of Communication for Development and Social Change, pp.1429–1438. Springer Singapore. [https://doi.org/10.1007/978-981-15-2014-3_96]
34. Velásquez Ramírez, M. G., Barrantes, J. A. G., Thomas, E., Gamarra Miranda, L. A., Pillaca, M., Tello Peramas, L. D. and Bazán Tapia, L. R., 2020. Heavy metals in alluvial gold mine spoils in the Peruvian Amazon. CATENA, 189, 104454. [https://doi.org/10.1016/j.catena.2020.104454]
35. Wang, B., Horna, V., Heckmann, M., Hapsari, K. A., Zimmermann, R. and Behling, H., 2023. Holocene environmental changes inferred from an oxbow lake in a Mauritia palm swamp (aguajal) in the Madre de Dios region, southeastern Peru. Review of Palaeobotany and Palynology, 312. [https://doi.org/10.1016/j.revpalbo.2023.104863]